

# Digital holographic microscopy by use of surface plasmon resonance for imaging of cell membranes

## Cuiying Hu

Jinan University  
Department of Optoelectronic Engineering  
Guangzhou 510632, China

## Jingang Zhong

Jinan University  
Department of Optoelectronic Engineering  
and  
Jinan University  
Key Laboratory of Optoelectronic Information  
and Sensing Technologies of Guangdong  
Higher Education Institutes  
Guangzhou 510632, China

## Jiawen Weng

Jinan University  
Department of Optoelectronic Engineering  
Guangzhou 510632, China

**Abstract.** A technique called surface plasmon resonance digital holographic microscopy (SPRDHM) for optical imaging of cell membranes is proposed. The intensity and phase distributions of the reflected light that is modulated by the cell membrane in surface plasmon resonance can be simultaneously obtained. The imaging principle and capability are theoretically analyzed and demonstrated by experiments. In addition, the technique is compared with total internal reflection digital holographic microscopy (TIRDHM) in theory and experiment, respectively. The results show that the SPRDHM technique is better in spatial resolution and phase sensitivity than the TIRDHM technique for imaging of cell membranes. © 2010 Society of Photo-Optical Instrumentation Engineers. [DOI: 10.1117/1.3497564]

Keywords: digital holography; microscopy; surface plasmon resonance; cell membrane imaging.

Paper 10022RR received Jan. 15, 2010; revised manuscript received Aug. 20, 2010; accepted for publication Aug. 26, 2010; published online Oct. 6, 2010.

## 1 Introduction

In cell biology, many key events in cellular trafficking occur at the cell membrane, and it is desirable to study these events by visualizing the cellular processes. Total internal reflection fluorescence microscopy (TIRFM) can be well suited for optical sectioning at cell-substrate regions with an unusually thin region (about half wavelength) of fluorescence excitation. It has been recognized that TIRFM can be the most powerful tool for studying events since it was demonstrated by Axelrod<sup>1</sup> in 1981. However, information on the morphology of cell membranes and the refractive index distribution of cell membranes, which are helpful to distinguish pathological cells from normal cells, cannot be achieved using the TIRFM technique.

Digital holography offers an excellent approach in obtaining quantitative intensity and phase information of a light-wave, and it has been utilized for microscopic imaging of microstructures and biological systems.<sup>2-6</sup> Ash and Kim,<sup>7</sup> who combined digital holography and total internal reflection (TIR), presented a technique termed total internal reflection digital holographic microscopy (TIRDHM), to obtain the image of a cell membrane.

Surface plasmon resonance microscopy (SPRM) is used as an analytical tool in biological and chemical sciences by detecting the refractive index distribution of sample surfaces. At present there are two kinds of SPRM. One is based on detecting the intensity of reflected light,<sup>8-10</sup> while the other is based on detecting the phase of reflected light.<sup>11,12</sup> However, the refractive index distribution of a sample surface cannot be uniquely determined from the intensity or phase images ob-

tained by this technique. The reason is that the intensity or phase of the reflected light is not a single-valued function of the refractive index for a fixed angle of incidence.

In this work, a surface plasmon resonance digital holographic microscopy (SPRDHM), which combines surface plasmon resonance (SPR) and digital holographic microscopy (DHM), is presented. DHM is applied to simultaneously obtain the quantitative intensity and phase of the reflected light that is modulated by the cell membrane in SPR. The refractive index distribution of the cell membrane can be uniquely determined using the quantitative intensity and phase distributions. In addition, the technique has been compared with the TIRDHM technique. The theory and experimental results show that SPRDHM is a potential tool for imaging of cell membranes.

## 2 Theory

### 2.1 Digital Holography

Digital holography in off-axis geometry is based on the classic holography principle, with the difference being that the hologram recording is performed by a charge-coupled device (CCD) camera and transmitted to a computer, and the subsequent reconstruction of the holographic image is carried out numerically by the computer.

Suppose that the coordinates of the hologram plane are  $(x_H, y_H)$ . The object and reference waves in the hologram plane are written as:

$$O(x_H, y_H) = O_0(x_H, y_H) \cdot \exp[j\phi(x_H, y_H)], \quad (1)$$

Address all correspondence to: Jingang Zhong, Jinan University, Department of Optoelectronic Engineering, Guangzhou, 510632, China Tel: 86-208-522-0484; Fax: 86-208-522-0414. E-mail: tzjg@jnu.edu.cn

$$R(x_H, y_H) = R_0 \cdot \exp[-j2\pi(\xi_r x_H + \eta_r y_H)], \quad (2)$$

where  $O_0(x_H, y_H)$  and  $R_0$  are the amplitudes of the object and the reference waves;  $j$  is the imaginary unit;  $\phi(x_H, y_H)$  is the phase of the object wave;  $\xi_r = \sin \theta_x / \lambda$  and  $\eta_r = \sin \theta_y / \lambda$  are the spatial frequencies of the reference wave in the  $x$  and  $y$  directions, respectively;  $\lambda$  is the wavelength of light; and  $\theta_x$  and  $\theta_y$  are the angles between the propagation direction of the object and the reference waves in the  $x$  and  $y$  directions, respectively.

The recorded intensity  $I(x_H, y_H)$  at the hologram plane is the square module of the amplitude superposition of the object and reference waves. It is given by:

$$\begin{aligned} I(x_H, y_H) &= |R(x_H, y_H) + O(x_H, y_H)|^2 = |R_0|^2 + |O_0(x_H, y_H)|^2 \\ &+ O_0(x_H, y_H)R_0 \exp\{j[2\pi(\xi_r x_H + \eta_r y_H) \\ &+ \phi(x_H, y_H)]\} + O_0(x_H, y_H)R_0 \exp\{-j[2\pi(\xi_r x_H \\ &+ \eta_r y_H) + \phi(x_H, y_H)]\}. \end{aligned} \quad (3)$$

The first two terms of Eq. (3) represent the intensities of the reference and object waves, respectively. They do not provide spatial information about the object optical field and form the zero-order term. The last two terms provide spatial frequency of the recorded hologram and are responsible for the virtual and real images, respectively.

The hologram is reconstructed by numerically propagating the optical field along the  $z$  direction in accordance with the Fresnel diffraction law. Cuche, Marquet, and Depeursinge<sup>13</sup> described the method used for hologram reconstruction in detail. The angular spectrum method has a significant advantage in that it has no minimum reconstruction distance requirement.<sup>14</sup> Therefore, it is fit for the analysis of the hologram of biological specimens by employing a microscope objective.

If  $E(x, y; 0)$  is the wavefront at plane  $z=0$ , the angular spectrum  $A(\xi, \eta; 0) = \mathcal{F}\{E(x, y; 0)\}$  at this plane is obtained by taking the Fourier transform, where  $\mathcal{F}\{\}$  denotes the Fourier transform;  $\xi$  and  $\eta$  are corresponding spatial frequencies of  $x, y$  directions, respectively; and  $z$  is the propagation direction of the object wave. The new angular spectrum  $A(\xi, \eta; d)$  at plane  $z=d$  is calculated from  $A(\xi, \eta; 0)$  as:

$$A(\xi, \eta; d) = A(\xi, \eta; 0) \cdot \exp\left\{j \frac{2\pi d}{\lambda} [1 - (\lambda\xi)^2 - (\lambda\eta)^2]^{1/2}\right\}. \quad (4)$$

The reconstructed complex wavefront at plane  $z=d$  is found by taking the inverse Fourier transform as

$$E(x, y; d) = \mathcal{F}^{-1}\{A(\xi, \eta; d)\}, \quad (5)$$

where  $\mathcal{F}^{-1}\{\}$  denotes the inverse Fourier transform. The intensity image  $I(x, y; d)$  and phase image  $\phi(x, y; d)$  are simultaneously obtained from a single digital hologram by calculating the square module of the amplitude and the argument of the reconstructed complex wavefront:

$$I(x, y; d) = |E(x, y; d)|^2, \quad (6)$$

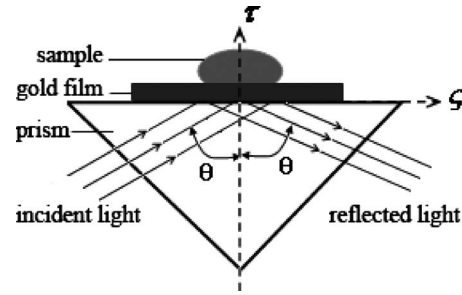


Fig. 1 The prism-based SPR configuration.

$$\phi(x, y; d) = \arctan\left(\frac{\text{imag}[E(x, y; d)]}{\text{real}[E(x, y; d)]}\right). \quad (7)$$

## 2.2 Surface Plasmon Resonance

Surface plasmons are electromagnetic waves associated with longitudinal oscillation of the free electrons on the interface between two media with dielectric constants of different signs, for example, between a noble metal (gold or silver) and air. The technique of surface plasmon resonance (SPR) uses the excited surface plasmons to probe biological and chemical information of the sample surface. The most widely used method by which to excite surface plasmon waves (SPWs) is prism-based attenuated total reflection. SPW is polarization dependent and is excited only by  $p$ -polarized waves. When  $p$ -polarized light is incident on the base of a prism with the angle of incidence greater than the critical angle of TIR, an evanescent field will extend from the prism into the noble metal. At a specific angle of incidence, the wave vector of the evanescent wave can match the wave vector of the SPW for a given frequency, and the SPR occurs. The specific angle of incidence is called the SPR angle. At this angle, the intensity of reflected light goes through a minimum, and the phase variation of reflected light is steepest due to surface plasmon resonance. The field associated with the surface plasmon, decaying exponentially, is sensitive to the change in the refractive index of the medium close to the metal-film surface.

The prism-based SPR configuration is shown as Fig. 1. It is composed of a prism, gold film, and a sample. The gold film is placed onto the prism's bottom surface, and the sample is attached to the surface of the gold film. The sequence of the optical media from prism to sample is denoted as 1, 2, 3. The symbols  $\zeta$  and  $\tau$  are the directions of the coordinate system. The reflectivity  $r$  of the light amplitude at the interface between two adjacent media is given by:<sup>15,16</sup>

$$r_{i,i+1}(\theta) = \frac{\xi_{i+1}(\theta) - \xi_i(\theta)}{\xi_{i+1}(\theta) + \xi_i(\theta)}, \quad (i = 1, 2), \quad (8)$$

$$\xi_i(\theta) = \frac{\varepsilon_i}{k_{\pi}(\theta)}, \quad (i = 1, 2, 3), \quad (9)$$

$$k_{\pi}(\theta) = \frac{2\pi}{\lambda} [\varepsilon_i - \varepsilon_0 \sin^2(\theta)]^{1/2}, \quad (i = 1, 2, 3), \quad (10)$$

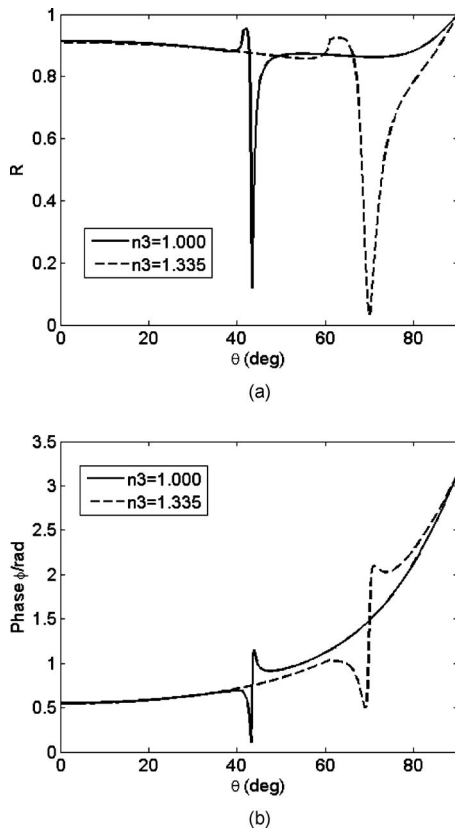


**Fig. 2** Relations between reflectivity  $R$ , reflection phase  $\phi$ , and the angle of incidence  $\theta$  in SPR with  $n_1=1.516$ : (a)  $R$  versus  $\theta$  and (b)  $\phi$  versus  $\theta$ .

$$\varepsilon_i \approx n_i^2, \quad (11)$$

where  $\theta$  is the angle of incidence;  $i$  denotes the  $i$ 'th optical medium;  $k_{\tau i}$  represents the wave number of the transmitted light in the  $i$ 'th optical medium along the  $\tau$  direction;  $\varepsilon_i$  is the dielectric constant of the  $i$ 'th optical medium; and  $n_i$  is refractive index of the  $i$ 'th optical medium.

The reflectivity of light amplitude in the SPR system is given as:<sup>15,16</sup>

$$r_{1,3}(\theta) = \frac{r_{1,2}(\theta) + r_{2,3}(\theta) \cdot \exp[j2d_2k_{\tau 2}(\theta)]}{1 + r_{1,2}(\theta)r_{2,3}(\theta) \cdot \exp[j2d_2k_{\tau 2}(\theta)]}, \quad (12)$$

where  $d_2$  is the thickness of the gold film. Therefore, the reflectivity  $R$  of light intensity and reflection phase  $\phi$  are expressed as:

$$R(\theta) = |r_{1,3}(\theta)|^2, \quad (13)$$

$$\phi = \arctan \left[ \frac{\text{imag}(r_{1,3})}{\text{real}(r_{1,3})} \right]. \quad (14)$$

Calculations are performed with  $n_1=1.516$  ( $n_1$  is the refractive index of the prism),  $n_2=-13.4+1.4j$  ( $n_2$  is the complex refractive index of the gold film),  $n_3=1.335$  or  $1.000$  ( $n_3$  is the refractive index of the sample), and  $\lambda=632.8$  nm to discuss the relations between reflectivity  $R$ , reflection phase  $\phi$ , and the angle of incidence  $\theta$ , according to Eqs. (13) and

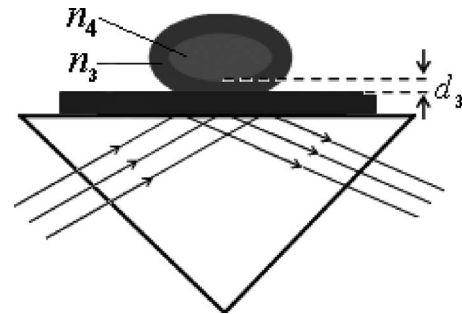


**Fig. 3** Schematic about the variation of refractive index in a sample.

(14). The thickness of the gold film  $d_2$  is 50 nm in the SPR configuration, which is the optimal value discussed by many researchers.<sup>15,17</sup>

Figure 2 shows the relations between  $R$ ,  $\phi$ , and  $\theta$  in SPR. It demonstrates that the SPR angles for  $n_3=1.000$  and  $n_3=1.335$  (the refractive index of a living cell is close to this value) are 43.6 and 71.4 deg, respectively. When the incident angle on the gold film/sample interface is close to 43.6 or 71.4 deg, there are evident changes both in the reflected light intensity and in its phase.

Physically, the changes of the reflected light in intensity and phase are due to the interaction between the lightwave and the delocalized electrons in gold film in the SPR technique. The states of the delocalized electrons are related to the dielectric constant  $\varepsilon_3$  of the sample near the gold film. Therefore, the change of  $\varepsilon_3$  can indirectly affect the intensity and phase of the reflected light. According to Eq. (11), the intensity and phase images obtained in the SPR technique can indirectly represent the refractive index distribution of sample near the gold film. When the incident angle is close to the SPR angle, the images are most sensitive to the variation of the refractive index of sample near the gold film.

Suppose that the sample can be divided into two layers, whose refractive indices are  $n_3=1.380$  and  $n_4=1.335$ , and  $d_3$  is the thickness of the medium with the refractive index  $n_3$ , as shown in Fig. 3. The relations between  $R$ ,  $\phi$ , and  $d_3$  are analyzed with  $n_1=1.67$ ,  $n_2=-13.4+1.4j$ , and  $\theta=60$  deg (close to the SPR angle) according to Eq. (8), with  $i=1,2,3$ , and Eqs. (9) and (10) with  $i=1,2,3,4$ , and the following equations:<sup>15</sup>

$$r_{i,4}(\theta) = \frac{r_{i,i+1}(\theta) + r_{i+1,4}(\theta) \cdot \exp[j2d_{i+1}k_{\tau i+1}(\theta)]}{1 + r_{i,i+1}(\theta)r_{i+1,4}(\theta) \cdot \exp[j2d_{i+1}k_{\tau i+1}(\theta)]}, \quad (i=1,2), \quad (15)$$

$$R(\theta) = |r_{1,4}(\theta)|^2, \quad (16)$$

$$\phi = \arctan \left[ \frac{\text{imag}(r_{1,4})}{\text{real}(r_{1,4})} \right]. \quad (17)$$

Figure 4 is a relation diagram between  $R$ ,  $\phi$ , and  $d_3$ . It indicates that the intensity and phase of the reflected light have a significant change when  $d_3$  is less than 100 nm, while there are almost no changes when  $d_3$  is larger than 100 nm. In other words, the intensity and phase of the reflected light are

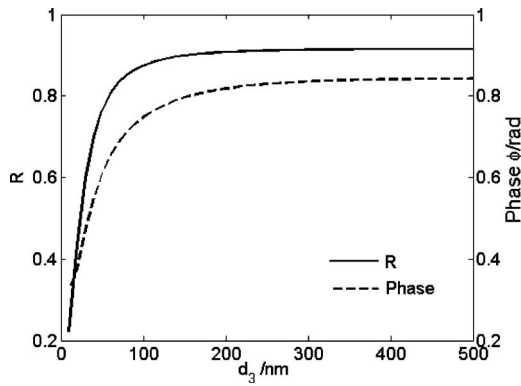


Fig. 4 Relation diagram between  $R$ ,  $\phi$ , and  $d_3$  in SPR.

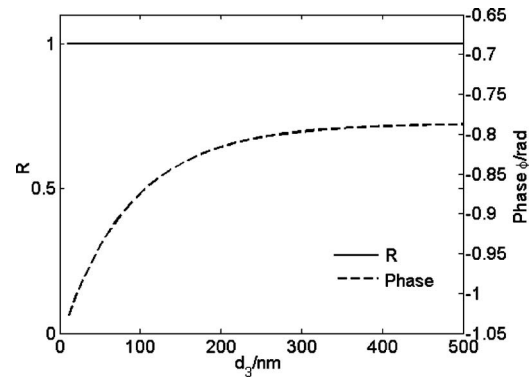


Fig. 6 Relation diagram between  $R$ ,  $\phi$ , and  $d_3$  in TIR.

affected by the medium with  $n_4$  when  $d_3$  is less than 100 nm. The intensity and phase images represent the refractive index distribution of a sample within about 100 nm near the gold film. Therefore, the spatial resolution in the vertical direction of the sample surface is about 100 nm, which is significantly less than a half wavelength for  $\lambda=632.8$  nm.

If the gold film is absent ( $d_2=0$ ), this corresponds to the TIR configuration. Figure 5 shows the relations between  $R$ ,  $\phi$ , and  $\theta$  in TIR, according to Eqs. (13) and (14). It demonstrates that the phase image can represent the refractive index distribution of a sample when the angle of incidence is greater than

the critical angle of TIR while the intensity image cannot represent the refractive index distribution. The phase sensitivity in the TIR technique is lower than that in the SPR technique at about the SPR angle. The relation diagram between  $R$ ,  $\phi$ , and  $d_3$  is shown in Fig. 6. It indicates that the phase of the reflected light has a significant change when  $d_3$  is less than 250 nm. Therefore, only the phase image can represent the refractive index distribution of a sample within about 250 nm near the prim surface. The spatial resolution in the vertical direction of the sample surface is about 250 nm, which is approximately a half wavelength. It is obvious that the SPR technique is better than the TIR technique in spatial resolution. The reason is that the evanescent wave is directly acting on the sample in the TIR technique, while it is indirectly acting on the sample through the gold film in the SPR technique.

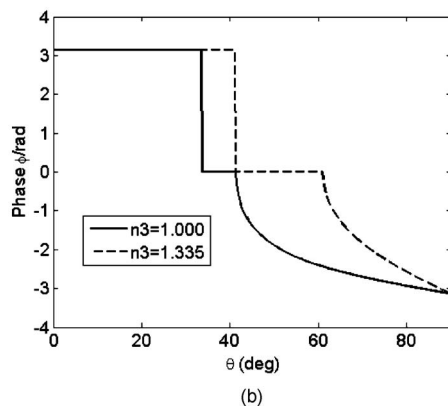
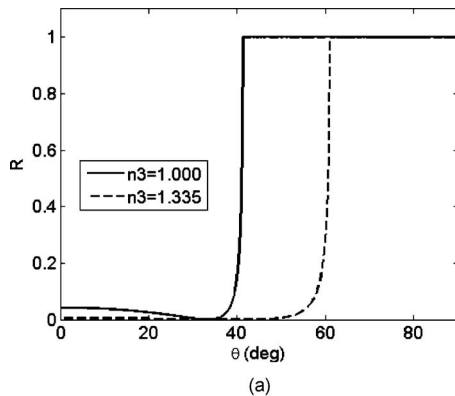


Fig. 5 The relations between reflectivity  $R$ , reflection phase  $\phi$ , and the angle of incidence  $\theta$  in TIR with  $n_1=1.516$ : (a)  $R$  versus  $\theta$  and (b)  $\phi$  versus  $\theta$ .

Biological or chemical information can be acquired by detecting the changes of the intensity or the phase of reflected light in SPRM. In the traditional SPRM detection method, the light intensity detection method has been studied extensively. However, the refractive index distribution of a sample near the gold film cannot be uniquely determined by the intensity of reflected light in SPRM, for the reason that the intensity of the reflected light is not a single-valued function of the refractive index at a fixed angle of incidence. Figure 7 shows the relations between reflectivity  $R$ , reflection phase  $\phi$ , and the refractive index  $n_3$  at an angle of incidence  $\theta=58$  deg with  $n_1=1.67$ . As shown in Fig. 7, the intensities at A and B are the same, but the refractive indices are different. Some prepara-

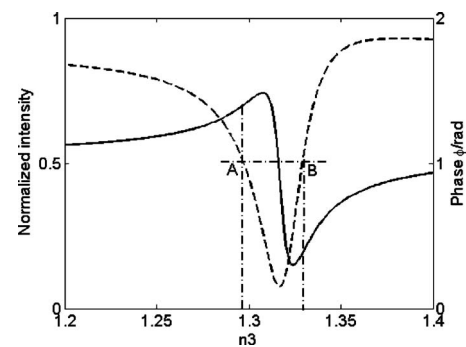
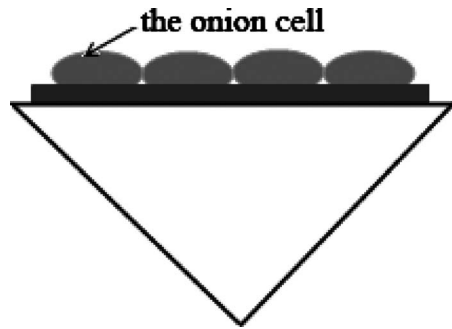


Fig. 7 Relations between  $R$ ,  $\phi$ , and the refractive index  $n_3$  at  $\theta=58$  deg with  $n_1=1.67$ .



**Fig. 8** Onion membrane placed on the gold film or the right-prism's bottom surface directly.

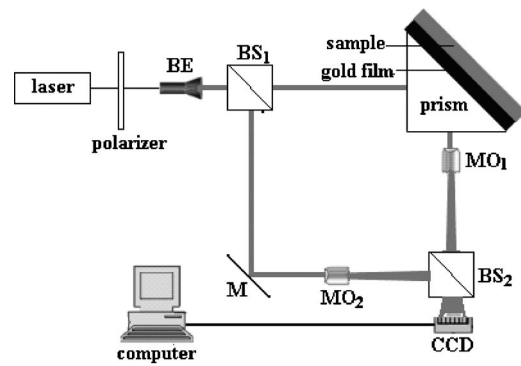
tory knowledge is necessary to judge which refractive index more reasonably corresponds to the same intensity.

Digital holography is applied to the SPR technique for reconstructing the wavefront of the reflected light to simultaneously obtain the intensity and phase images of the sample. From the reconstructed complex wavefront, the intensity and phase images can be simultaneously obtained according to Eqs. (6) and (7).

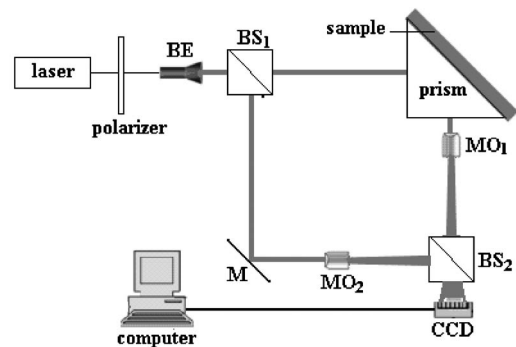
### 3 Experiments and Results

Experiments of the SPRDHM technique are performed. The samples in the experiments are onion cells from the inner surface of an onion. The onion cells are flat on the gold film in the SPRDHM technique, or the prism's bottom surface in the TIRDHM technique, as shown in Fig. 8. To utilize SPR properly, SPRDHM experiments should be performed near the SPR angle. The refractive index of air is about 1.000, and the refractive index of a cell is close to 1.335. The SPR angles for air and cell are different. Therefore, we implemented two different experiments corresponding to the SPR angles of air and cell.

First, the experiments in which the incident angle is near the SPR angle of air are performed employing the apparatus depicted in Fig. 9. The SPR angle of air is about 43.6 deg for the prim with  $n_1=1.516$ . The optical arrangement is analogous to a Mach-Zehnder interferometer. The incident angle is around 45 deg, which is very close to 43.6 deg. A light beam from a He-Ne laser ( $\lambda=632.8$  nm) passes through a polarizer. We adjust the direction of the polarizer until a  $p$ -polarized light is outgoing. The  $p$ -polarized light, expanded and collimated by BE, is split into two beams by a beamsplitter prism  $BS_1$ . One beam, serving as the object beam, illuminates a transparent onion membrane at about a 45-deg angle. The other serves as a reference beam. A beamsplitter  $BS_2$  placed in front of a CCD camera [Mintron (Fremont, California) 22K9HC,  $795 \times 596$  pixels,  $8.33 \times 8.33 \mu\text{m}^2$  per pixel] combines the two beams, and the holograms are recorded by the CCD camera with 8-bit gray scale output. The slight angle is introduced between the object and the reference beams by tilting the beamsplitter  $BS_2$  for the off-axis holography. A microscope objective  $MO_1$  ( $4\times$ , 0.1 NA) is employed to produce a magnified image of the sample, and another  $MO_2$  ( $4\times$ , 0.1 NA) is placed in the reference arm to get the matching wavefront curvature.



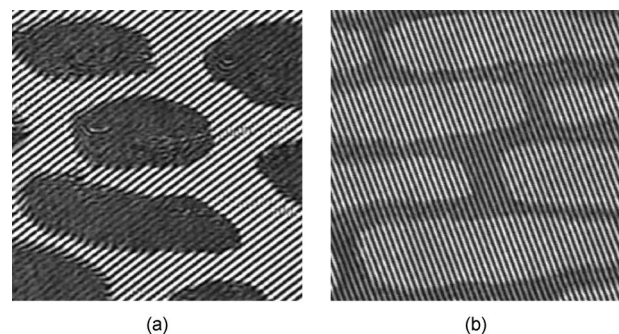
(a)



(b)

**Fig. 9** Apparatus for digital holographic experiment: (a) SPRDHM and (b) TIRDHM.

Figures 10(a) and 10(b) show the holograms of onion specimens obtained by TIRDHM and SPRDHM techniques, respectively. In the experiment, the sample plane will optically appear to the camera at an angle of inclination, which is equal to the angle of incidence. Therefore, the images obtained by the camera will be compressed in one direction. The image area is  $184 \times 130 \mu\text{m}^2$  (the images are compressed to 0.72 times in the  $x$  direction), recorded at  $256 \times 256$  pixels. The interference fringes on the cell surface in Fig. 10(a) are very blurred; the reason is that the angle is less than the critical angle of TIR, and there is a low reflectivity from the prism/cell interface. The blurred fringes lead to difficulties in the digital reconstruction for a hologram. The interference fringes on the cell surface in Fig. 10(b) are clear because of



(a)

(b)

**Fig. 10** The holograms of onion specimens obtained by TIRDHM and SPRDHM techniques, respectively: (a) TIRDHM and (b) SPRDHM.

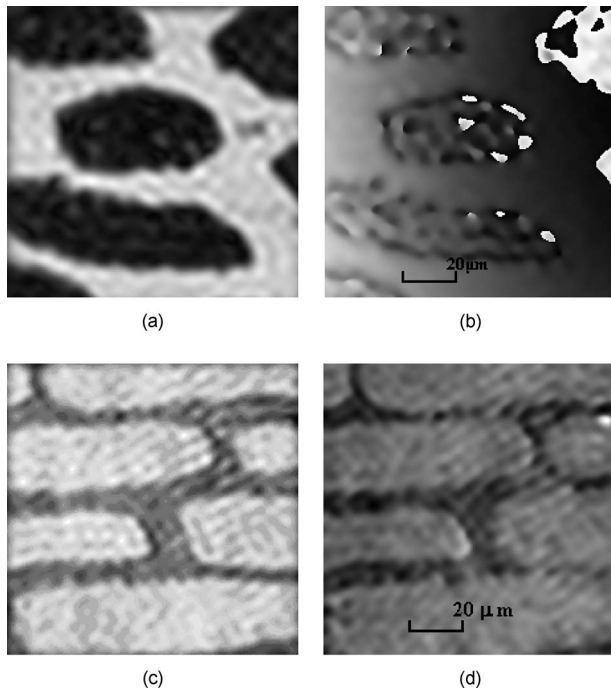


**Fig. 11** Reconstructed images of the holograms in Fig. 10. (a) and (b) are the reconstructed intensity and phase images corresponding to Fig. 10(a). (c) and (d) are the reconstructed intensity and phase images corresponding to Fig. 10(b).

the higher reflectivity shown in Fig. 2(a). Figures 11(a) and 11(b) show the reconstructed intensity and phase images obtained by the TIRDHM technique, respectively. It is obvious that some errors are introduced by the blurred interference fringes. Figures 11(c) and 11(d) show the reconstructed intensity and phase images obtained by the SPRDHM technique, respectively. Figures 12(a) and 12(b) are the 3-D views of Figs. 11(c) and 11(d). Figures 13(a) and 13(b) are graphs of cross sections of the normalized intensity and phase profiles along column 65 in Figs. 11(c) and 11(d), respectively. Therefore, the incident angle of light must be greater than the critical angle of the TIR to cell medium in the TIRDHM technique, while the incident angle of light can be close to the SPR angle of air in the SPRDHM technique. When the prism is placed at one corner, as shown in Fig. 9, the incident angle is around 45 deg, that is, the angle is close to the SPR angle of air at 43.6 deg. The system is very convenient for us to perform digital holographic experiments.

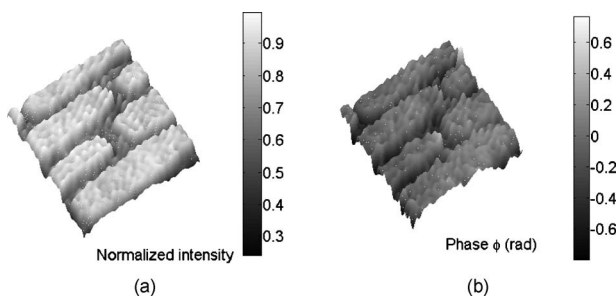


**Fig. 12** 3-D views of Figs. 11(c) and 11(d).

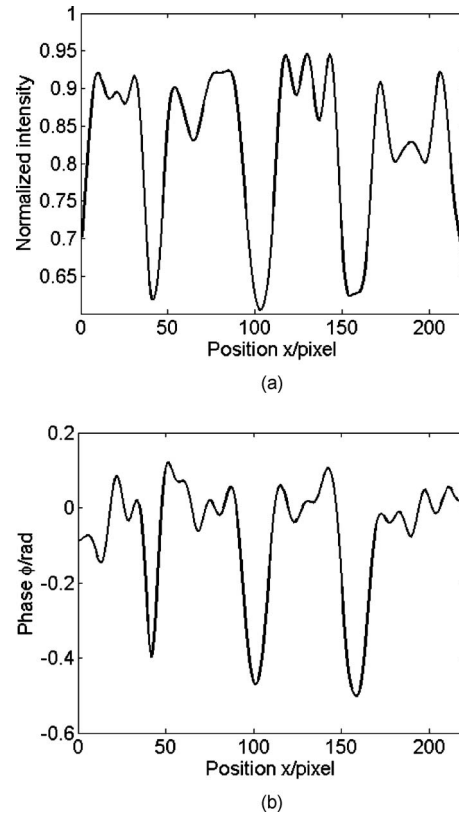


**Fig. 13** Graphs of cross sections along column 65 in Figs. 11(c) and 11(d): (a) corresponding to Fig. 11(c) and (b) corresponding to Fig. 11(d).

The other experiment, in which the incident angle is near the SPR angle of the cell, is performed by employing the apparatus depicted in Fig. 14. The SPR angle of the cell (if the refractive index of the cell is close to 1.335) is about 71.4 deg for the prism with  $n_1=1.516$ . At 71.4 deg, the images will be compressed 0.32 times in one direction. Therefore, a prism with higher refractive index  $n_1=1.67$  is used in the experiment to get a smaller SPR angle 58 deg for  $n_3=1.335$ , so that the compression can be reduced. At this angle, the images will be compressed 0.53 times in one direction. There are four

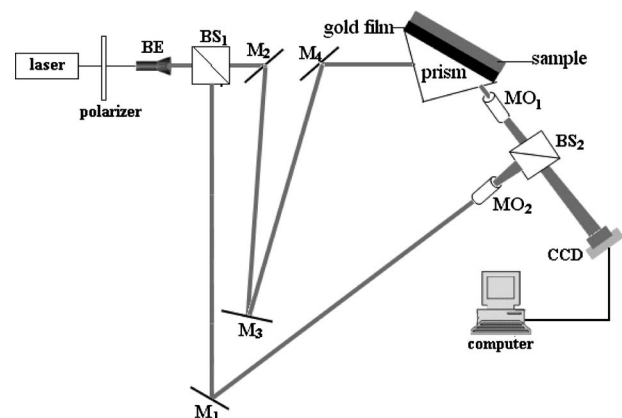


**Fig. 14** Apparatus for the SPRDHM experiment at a bigger SPR angle.

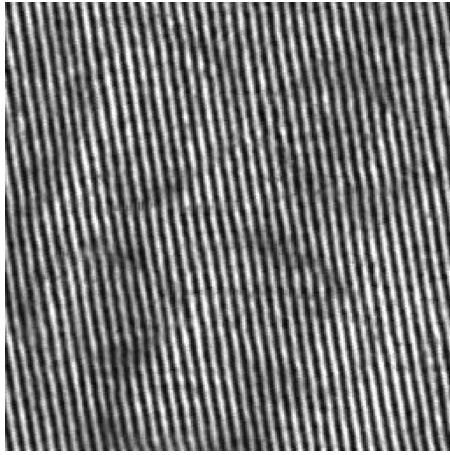


Fig. 15 Hologram of another onion specimen.

mirrors in the optical system, among which  $M_1$ ,  $M_2$ , and  $M_3$  are used to match the optical path of an object beam with the one of the reference beam. Figure 15 shows the hologram of another onion specimen. The image area is  $190 \times 100 \mu\text{m}^2$ . The reconstructed images are shown in Fig. 16. Figures 17(a) and 17(b) are graphs of cross sections of the normalized intensity and phase profile along row 150 in Figs. 16(a) and 16(b), respectively. The quantitative intensity and phase images can indirectly represent the refractive index distribution of cell membranes near the gold film.

#### 4 Conclusion

A new technique termed SPRDHM is introduced in this research. The technique combines SPR and DHM to simultaneously obtain the intensity and phase images of cell membranes. The quantitative intensity and phase images can indirectly represent the refractive index distribution of cell

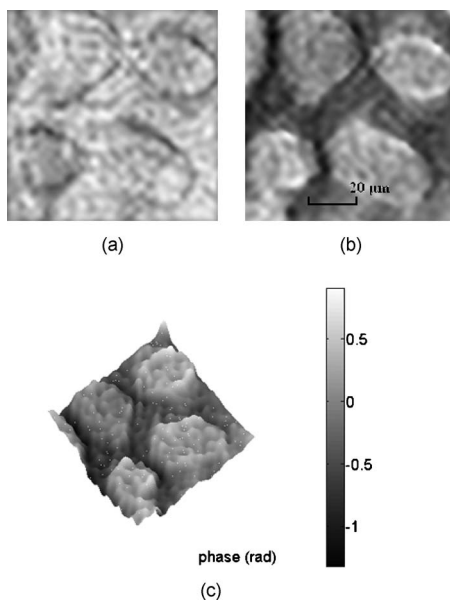


Fig. 16 Reconstructed images of the hologram in Fig. 15. (a) The reconstructed intensity image. (b) The reconstructed phase image.

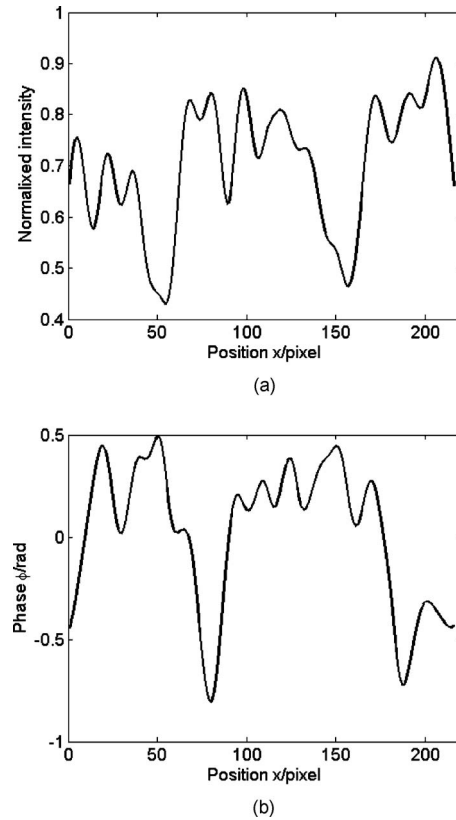


Fig. 17 Graphs of cross sections along row 150 in Fig. 16: (a) corresponding to Fig. 16(a) and (b) corresponding to Fig. 16(b).

membrane near the gold film. The contrast experiments with onion specimens are performed using the TIRDHM and SPRDHM techniques under the same condition. The results show that the SPRDHM technique possesses the imaging capability of simultaneously obtaining the intensity and phase images of cell membrane, while only quantitative phase images can be obtained using the TIRDHM technique. The SPRDHM technique is better than the TIRDHM technique in spatial resolution and phase sensitivity for imaging of cell membrane. Therefore, SPRDHM has a potential advantage in biological cellular microscopy and surface science.

#### Acknowledgment

This work was supported by National Natural Science Foundation of China under grant number 60677019.

#### References

1. D. Axelrod, "Cell-substrate contacts illuminated by total internal reflection fluorescence," *J. Cell Biol.* **89**, 141–145 (1981).
2. B. Kemper and G. von Bally, "Digital holographic microscopy for live cell applications and technical inspection," *Appl. Opt.* **47**, A52–A61 (2008).
3. P. Langehanenberg, B. Kemper, D. Dirksen, and G. von Bally, "Autofocusing in digital holographic phase contrast microscopy on pure phase objects for live cell imaging," *Appl. Opt.* **47**, D176–D182 (2008).
4. J. Kühn, F. Montfort, T. Colomb, B. Rappaz, C. Moratal, N. Pavillon, P. Marquet, and C. Depeursinge, "Sub-micrometer tomography of cells by multiple-wavelength digital holographic microscopy in reflection," *Opt. Lett.* **34**, 653–655 (2009).
5. K. Jeong, L. Peng, J. J. Turek, M. R. Melloch, and D. D. Nolte,

- “Fourier-domain digital holographic optical coherence imaging of living tissue,” *Appl. Opt.* **46**, 4999–5008 (2007).
6. L. Xu, X. Peng, J. Miao, and A. K. Asundi, “Studies of digital microscopic holography with applications to microstructure testing,” *Appl. Opt.* **40**, 5046–5051 (2001).
  7. W. M. Ash and M. K. Kim, “Digital holography of total internal reflection,” *Opt. Express* **16**, 9811–9820 (2008).
  8. C. T. Campbella and G. Kim, “SPR microscopy and its applications to high-throughput analyses of biomolecular binding events and their kinetics,” *Biomaterials* **28**, 2380–2392 (2007).
  9. R. Thariani and P. Yager, “Novel, high-quality surface plasmon resonance microscopy,” *Sens. Actuators B* **130**, 765–770 (2008).
  10. J. S. Shumaker-Parry, R. Aebersold, and C. T. Campbell, “Parallel, quantitative measurement of protein binding to a 120-element double-stranded DNA array in real time using surface plasmon resonance microscopy,” *Anal. Chem.* **76**, 2071–2082 (2004).
  11. Y. Xinglong, W. Dingxin, W. Xing, D. Xiang, L. Wei, and Z. Xinsheng, “A surface plasmon resonance imaging interferometry for protein micro-array detection,” *Sens. Actuators B* **108**, 765–771 (2005).
  12. R. Y. He, Y. D. Su, G. L. Chang, and S. J. Chen, “Imaging the cell membrane with surface plasmon resonance phase microscopy,” *Proc. SPIE* **6324**, 632409 (2006).
  13. E. Cucho, P. Marquet, and C. Depeursinge, “Simultaneous amplitude-contrast and quantitative phase-contrast microscopy by numerical reconstruction of Fresnel off-holograms,” *Appl. Opt.* **34**, 6994–7001 (1999).
  14. L. Yu and M. K. Kim, “Wavelength-scanning digital interference holography for tomographic three-dimensional imaging by use of the angular spectrum method,” *Opt. Lett.* **30**, 2092–2094 (2005).
  15. X. Caide and S. F. Sui, “Characterization of surface plasmon resonance biosensor,” *Sens. Actuators B* **66**, 174–177 (2000).
  16. S. J. Chen, Y. D. Su, F. M. Hsiu, C. Y. Tsou, and Y. K. Chen, “Surface plasmon resonance phase-shift interferometry: real-time DNA microarray hybridization analysis,” *J. Biomed. Opt.* **10**(3), 034005 (2005).
  17. Y. Xinglong, W. Dingxin, and Y. Zibo, “Simulation and analysis of surface plasmon resonance biosensor based on phase detection,” *Sens. Actuators B* **91**, 285–290 (2003).